Optomechanical devices based on traveling-wave microresonators

Yan-Lei Zhang, [1,2], Chun-Hua Dong, [1,2], Chang-Ling Zou, [1,2,3],*
Xu-Bo Zou, [1,2],† Ying-Dan Wang, [4,5], and Guang-Can Guo [1,2]
[1] *Key Laboratory of Quantum Information, University of Science and Technology of China, Hefei, 230026, People's Republic of China;*
[2] *Synergetic Innovation Center of Quantum Information & Quantum Physics, University of Science and Technology of China, Hefei, Anhui 230026, China*
[3] *Department of Applied Physics, Yale University, New Haven, CT 06511, USA*
[4] *CAS Key Laboratory of Theoretical Physics, Institute of Theoretical Physics, Chinese Academy of Sciences, P.O. Box 2735, Beijing 100190, China and*
[5] *School of Physical Sciences, University of Chinese Academy of Sciences, No.19A Yuquan Road, Beijing 100049, China*
(Dated: February 7, 2017)

We theoretically study the unique applications of optomechanics based on traveling-wave microresonators, where the optomechanical coupling of degenerate modes can be enhanced selectively by optically pumping in different directions. We show that the unique features of degenerate optical modes can be applied to the entangled photon generation of clockwise and counter-clockwise optical modes, and the nonclassicality of entangled photon pair is discussed. The coherent coupling between the clockwise and counter-clockwise optical mods and two acoustic modes is also studied, in which the relative phase of the optomechanical couplings plays a key role in the optical non-reciprocity. The parity-time symmetry of acoustic modes can be observed in the slightly deformed microresonator with the interaction of forward and backward stimulated Brillouin Scattering in the triple-resonance system. In addition, the degenerate modes are in the decoherence-free subspace, which is robust against environmental noises. Based on parameters realized in recent experiments, these optomechanical devices should be readily achievable.

PACS numbers: 42.50.Wk, 42.50.Ex, 07.10.Cm, 11.30.Er

arXiv:1702.01500v1 [quant-ph] 6 Feb 2017

I. INTRODUCTION

Optomechanical devices [1–5] have attracted considerable attentions in integrated photonic circuits [6–8], memory [9, 10] and high precision measurements [11–13] for practical applications. There are also excellent test bed for investigating the quantum behaviors at macroscopic level [20] and are attractive for fundamental studies on physics, such as the gravitational wave detection [1, 14, 15], quantum-to-classical transitions [16, 17], and quantum information processing [18, 19]. In past few years, many remarkable progresses have been achieved both in theory and experiment, such as ground state cooling of the mechanical resonator [21], optomechanically induced transparency [22, 23], optomechanical entanglement [24] and squeezing [25], and optical frequency conversion [26, 27].

Recently, more and more studies on multimode optomechanics (MOM) [1] have been carried out, for more functional devices and applications. Because they provide more degrees of freedom, people can realize new phenomena that are not possible in single mode optomechanical systems, such as the optical non-reciprocity [28–30], parity-time symmetry [31], chiral symmetry breaking [32], and topological energy transfer [33]. Different from the triple-resonance enhanced optomechanical interaction [34, 35], the MOM in this paper is referring to more than one optical signal mode or mechanical mode. Many schemes [19, 36–38] have been proposed to realize the MOM [39] based on the coupled cavities or hybrid optomechanical systems. However, in practical physical systems, it is challenging to fabricate multiple optical or mechanical resonators that have the frequencies matching each other. In additional to the frequency mismatching problem, the MOM also requires complex design for the efficient coupling between separated resonators.

In this paper, we propose to use the traveling-wave microresonators to explore the MOM, which allows many potential new phenomena and applications. The whispering-gallery microcavities [26, 40–42, 44–46] is one of the candidate systems, which supports degenerate clockwise (CW) and counter-clockwise (CCW) traveling-wave modes, which have already been used in optomechanically induced non-reciprocity [47–50]. By using the degenerate oppositely propagating optical modes, we demonstrate the entangled photon generation and the controllable optical non-reciprocity. The CW and CCW acoustic waves also enable the study of the non-Hermitian dynamics of phonons, and the parity-time symmetry of acoustic modes is proposed in the slightly deformed traveling-wave microresonator. The traveling-wave microresonator provides an excellent platform for studying the optomechanics with multiple degrees of freedom, and the schemes proposed in this work are feasible for experiments. The integration of all modes in single solid state microresonator also holds the great advantage that the noise of degenerate CW and CCW traveling-

*Electronic address: clzou321@ustc.edu.cn
†Electronic address: xbz@ustc.edu.cn

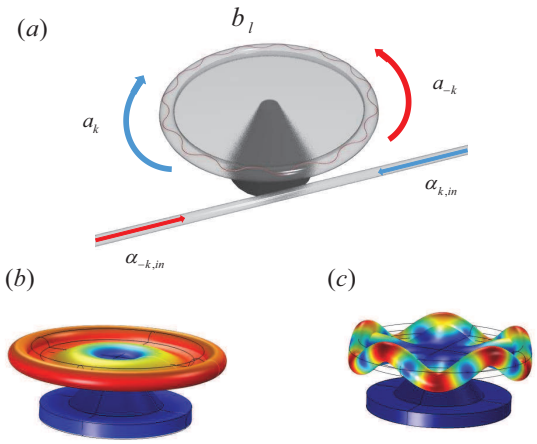

FIG. 1: (Color online) (a) Schematic of the the travelling-wave multimode optomechanical system. Here a_k and a_{-k} are the annihilation operators of the clockwise (CW) and counter-clockwise (CCW) traveling-wave modes, and b_l is the annihilation operator of the mechanical mode. (b) The breath mechanical mode $l = 0$ for dispersive optomechanics. (c) The Brillouin mechanical mode $l = 5$ for triple-resonant optomechanics.

wave modes could cancel each other, where the mode pair actually forms a decoherence-free subspace, which makes optomechanical devices robust against environmental noises and holds great potential for applications in quantum information processing.

The paper is organized as follows. In Sec. II, we show the CW and CCW traveling-wave modes in traveling-wave microresonators, and develop the Hamiltonian description of the MOM. Based on this model, we propose three unique applications in this system: the entangled photon generation of CW and CCW modes in Sec. III, the non-reciprocal conversion between CW and CCW optical modes in Sec. IV, and the phononic parity-time symmetry in Sec. V. Based on parameters realized with existing technology in recent experiments, these optomechanical devices should be readily achievable. We give a discussion about the potential advantages of the traveling-wave optomechanical system in In Sec. VI, and then summarize in Sec. VII.

II. THE SYSTEM

In this work, we consider an MOM system as shown in Fig. 1 (a): an integrated non-magnetic dielectric microresonator served as both optical and mechanical resonator. The microresonator possesses the rotational symmetry, leading to the degeneracy of the optical or mechanical modes that are propagating in the CW and the CCW directions. In general, the Hamiltonian description of the system can be written as

$$H = H_0 + H_i + H_d, \tag{1}$$

in which ($\hbar = 1$)

$$H_0 = \sum_{k=-N}^{N} \omega_{c,k} a_k^\dagger a_k + \sum_{l=-M}^{M} \omega_{m,l} b_l^\dagger b_l \tag{2}$$

is the system Hamiltonian, which describes the optical and mechanical modes. Due to the rotational symmetry, both optical and mechanical mode fields can be represented by the traveling field $\overrightarrow{E}_k(r,z)\, e^{-ik\phi}$ and $\overrightarrow{u}_l(r,z)\, e^{-il\phi}$, with r, z, ϕ representing the cylindrical coordinator, k and l are the azimuthal quantum numbers. Therefore, we use a_k and b_l as the annihilation operators of the k-th optical and l-th mechanical modes, and the $\omega_{c,k}$ and $\omega_{m,l}$ are the corresponding mode frequencies. As mentioned above, we have $\omega_{c,k} = \omega_{c,-k}$ and $\omega_{m,l} = \omega_{m,-l}$ due to the CW and CCW symmetry.

The mechanical motion of the dielectric microresonator can modify the optical mode frequency, through the geometry effect and the photo-elastic effect [41, 42], which leads to the optomechanical interaction Hamiltonian as

$$H_I = \sum_{j,k,l} g_{j,k,l} \left(a_j + a_j^\dagger\right)\left(a_k + a_k^\dagger\right)\left(b_l + b_l^\dagger\right). \tag{3}$$

The coupling strength $g_{j,k,l}$ is determined by the overlap of the optical electric field and the mechanical displacements or strain [41–43]. Since the integral $\int d\phi e^{-i(j+k+l)\phi} = \delta(j+k+l)$, the optomechanical interaction in this traveling-wave microresonator should satisfy the selection rule that $j \pm k \pm l = 0$. We can separate the interaction Hamiltonians into two categories:

1. Dispersive optomechanics as shown in Fig. 1 (b).

$$H_{I,1} = \sum_k g_{k,k,0} a_k^\dagger a_k \left(b_0 + b_0^\dagger\right). \tag{4}$$

Here, $g_{k,k,0}$ is the single-photon coupling rate, which corresponds to the optical cavity frequency shift per phonon excitation. This dispersive optomechanics indicates the mechanical motion shifts the optical mode frequency. Due to the selection rule, only the mechanical mode with $l = 0$, i.e. the breath-type modes [22, 47] can give rise to such interaction.

2. Triple-resonant optomechanics as shown in Fig. 1 (c).

$$H_{I,2} = \sum_{j,k} g_{j,k,j-k} \left(a_j^\dagger a_k b_{j-k} + a_j a_k^\dagger b_{j-k}^\dagger\right). \tag{5}$$

It describes a Brillouin scattering in this triple-resonant system [50], where a photon in mode j split into a photon in mode k and a phonon in mode $j-k$. Here, $g_{j,k,l}$ is the Brillouin scattering coupling strength, which is non-zero only when the energy ($\omega_m = \omega_{c,j} - \omega_{c,k}$) and momentum ($l = j - k$) conservation are satisfied.

The term H_d describes the driving of the optical modes and also the optical signal input to the system. With the weak interaction coupling, we can use strong optical driving fields to enhance optomechanical coupling strength [26, 50], and the optomechanical system evolves by optical signal input.

III. DEGENERATE PHOTON PAIR GENERATION

For dispersive optomechanics, we can choose the two degenerate CCW ($-k$) and CW (k) optical modes that are coupled to the breath mechanical mode, thus the interaction Hamiltonian is

$$H = g_{k,k,0}\left(a_k^\dagger a_k + a_{-k}^\dagger a_{-k}\right)\left(b_0 + b_0^\dagger\right). \tag{6}$$

The system is a general bosonic three-mode system, as shown in the Fig. 2(a). Such model can also be realized in a ring type resonator coupling to a local mechanical oscillator [1]. Since both a_k and a_{-k} can coherently couple with the mechanical mode, it is possible to realize the interaction between a_k and a_{-k} mediated by the mechanical mode. It has been demonstrated that the red-detuned laser pump on both CW and CCW direction can induce the effective coupling between the CW and CCW signal photons. If we pump one direction with blue detuned laser, there will generate a photon-phonon pair (anti-Stokes process), and the red detuned laser on the other direction will convert the phonon to photon (Stokes process), thus generate entangled photons propagate in opposite directions.

To study the entangling interaction between CW and CCW signal photons, we assume two driving fields of the CW and CCW optical modes with frequency detuned from the cavity as $\Delta_{d,k'} = \omega_{d,k'} - \omega_{c,k'}$, with $k' = \pm k$, where $\omega_{d,k'}$ is the drive laser frequency. Let the detuning $-\Delta_{d,k} = \Delta_{d,-k} = \omega_m$, and apply the standard linearization treatment, the effective Hamiltonian can be written as

$$\begin{aligned} H_{lin} =& -\Delta_{d,\mathrm{k}} a_\mathrm{k}^\dagger a_k - \Delta_{d,-\mathrm{k}} a_{-\mathrm{k}}^\dagger a_{-\mathrm{k}} + \omega_m b_0^\dagger b_0 \\ &+ G_\mathrm{k}\left(a_\mathrm{k}^\dagger b_0 + a_\mathrm{k} b_0^\dagger\right) + G_{-\mathrm{k}}\left(a_{-k}^\dagger b_0^\dagger + a_{-\mathrm{k}} b_0\right). \end{aligned} \tag{7}$$

Here, the coupling strength $G_{\mathrm{k}(-\mathrm{k})} = g_{k,k,0}\alpha_{\mathrm{k}(-\mathrm{k})}$ is enhanced by the driving field amplitude $\alpha_{\mathrm{k}(-\mathrm{k})}$. , The rotating wave approximation has been applied above with the assumption $\omega_m \gg G_{k(-\mathrm{k})},\ \kappa,\ \gamma_m$, where κ and γ_m are the cavity and mechanical damping rates, respectively.

For studying the entanglement of the photon pair, a weak signal is sent into CW optical mode as

$$H_s = i\sqrt{\kappa_{in}}\epsilon_{s,k}\left(a_\mathrm{k}^\dagger e^{-i(\omega_s-\omega_{d,\mathrm{k}})t} - H.c.\right), \tag{8}$$

where κ_{in} is the external coupling to the cavity. The dynamics of the density matrix (ρ) of the system is governed by the Master equation [51], which reads

$$\begin{aligned} \frac{d\rho}{dt} =& -i\left[H_{lin} + H_s, \rho\right] + \kappa\left[\mathcal{L}\left(a_\mathrm{k}\right) + \mathcal{L}\left(a_{-k}\right)\right] \\ &+ \left(n_{th}+1\right)\gamma_m \mathcal{L}\left(b_0\right) + n_{th}\gamma_m \mathcal{L}\left(b_0^\dagger\right), \end{aligned} \tag{9}$$

where $\mathcal{L}(A) = A\rho A^\dagger - \left(A^\dagger A\rho + \rho A^\dagger A\right)/2$ is the Lindblad superoperator for any operator A, and n_{th} is the phonon thermal excitation. In our calculation, we choose the damping rate of optical mode $\kappa/2\pi = 15\,\mathrm{MHz}$, the damping rate of mechanical mode $\gamma_m/2\pi = 22\,\mathrm{kHz}$, and $\kappa_{in} = \kappa/2$ from the experimental parameters [47].

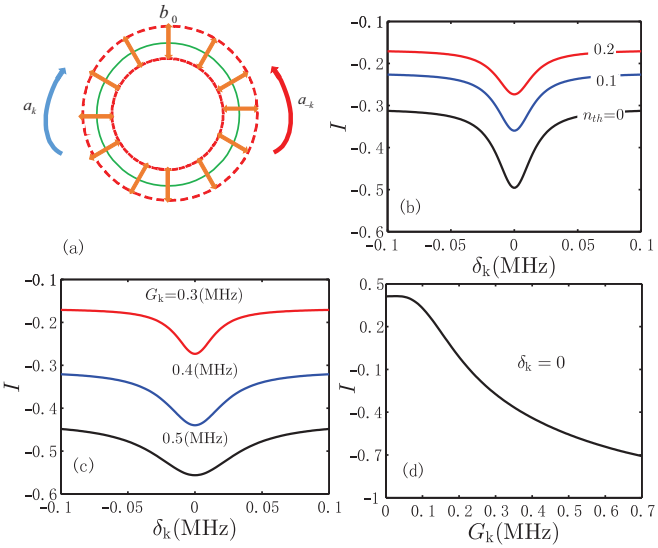

FIG. 2: (Color online) (a) Schematic diagram of entangled photon generation. (b) The parameter I as a function of the detuning δ_k for $G_\mathrm{k}/2\pi = 0.3$ MHz and $n_{th} = 0,\ 0.1,\ 0.2$. (c) The parameter I as a function of the detuning δ_k for $n_{th} = 0.2$ and $G_k/2\pi = 0.3\ 0.4,\ 0.5$ MHz. (d) The parameter I as a function of the effective coupling G_k for the detuning $\delta_\mathrm{k} = 0$ and $n_{th} = 0.2$. Other parameters are $G_{-\mathrm{k}}/2\pi = 0.1$ MHz and $\epsilon_{s,k} = 0.1$ MHz.

To characterize the nonclassicality of the two-mode field, we introduce the parameter [52]

$$I = \frac{\sqrt{\left\langle a_\mathrm{k}^{\dagger 2} a_\mathrm{k}^2\right\rangle \left\langle a_{-\mathrm{k}}^{\dagger 2} a_{-\mathrm{k}}^2\right\rangle}}{\left\langle a_k^\dagger a_\mathrm{k} a_{-k}^\dagger a_{-\mathrm{k}}\right\rangle} - 1, \tag{10}$$

as a measure. For coherent states, $I = 0$, while for nonclassical states we will have $I < 0$ [52, 53].

In the Fig. 2, we numerically investigate the nonclassical parameter I of the system in equilibrium state for various n_{th} and G_k. We should notice that the blue-detuned drive produces the photon-phonon pairs, and it would also induce instability of the system due to the amplification. Using the well-known Routh-Hurwitz stability conditions [54], we derive the necessary and sufficient

stability condition for this model as $G_{\rm k}^2 - G_{-k}^2 > -\kappa\gamma/4$. In experiment, we can adjust the drive amplitude to guarantee $G_{-\rm k}^2 < \kappa\gamma/4$, therefore the system is always stable for arbitrary $G_{\rm k}$.

The nonclassicality parameters I as a function of the detuning $\delta_{\rm k} = \omega_s - \omega_{c,k}$ for various thermal phonon n_{th} are plotted in Fig. 2(b). As expected, the nonclassicality parameter shows negativity $I < 0$, which implies nonclassicality of the two oppositely propagating fields due to the two drivings. When the detuning $\delta_{\rm k} = 0$, the nonclassicality parameter reaches the smallest value. For more thermal phonon excitation n_{th}, more noise phonon is converted to signal mode, thus the nonclassicality reduces. This noise phonon conversion can also actually be suppressed with the increasing of the effective coupling G_k, as shown in Fig. 2(c) that the nonclassicality is improved for larger G_k. This is because when the effective coupling $G_{\rm k}$ increases, the cooling of the phonon mode can be enhanced, and the thermal noise is suppressed [1]. As shown in Fig. 2(d), we plot the nonclassicality parameter I as a function of $G_{\rm k}$ at the detuning $\delta_k = 0$. The I reduces with the coupling $G_{\rm k}$ and approaches -1, which is the lower bound of the parameter I.

The degenerate CW and CCW signal photons travel in opposite directions, thus the two mode can be separately coupled to different optical waveguides [as shown in Fig. 1(a)], which enable the type-II (spatially separable) entanglement photon source on a photonic chip. Compared to the crystals used in free space parametric down conversion, the traveling-wave optomechanical approach has the advantages that narrow linewidth, long coherence time, high purity and waveguide integrated. This scheme can be used to realize quantum repeaters [55] and nonclassical interference [56] by using indistinguishable photon pair generated by the integrated microresonator. The potential limitation of the thermal phonon n_{th} can be relaxed by coupling the mechanical mode to a third optical cavity mode, which is used to cool the mechanical mode towards the ground state. When the damping rates satify $\gamma_m \gg \kappa$, the steady-state entanglement can be achieved via reservoir engineering [57, 58]. For large mechanical noise $n_{th} \gg 0$, quantum interference can be applied to achieve robust photon entanglement [59] in the strong coupling regime $G > \kappa$.

IV. PHASE-CONTROLLED NON-RECIPROCITY

As shown in Fig. 1(a), the signal photon propagating in the forward and backward directions is coupling to the CCW and CW modes, therefore directional pump to the system can induce transmission difference between the forward and backward signal in the waveguide, which leads to the optical non-reciprocity. Different from the single mechanical mode induced nonreciprocity demonstrated in Ref. [47, 48], here we propose a new scheme for phase-controlled non-reciprocal conversion by two mechanical mode. The underlying mechanism is that the two mechanical modes allow the paths for the coupling between the oppositely propagating signals, and effective coupling can be controlled by changing the relative phase of the two paths, which eventually leads to the one-way conversion between two modes.The schematic of the scheme is shown in Fig. 3(a), where the CW and CCW modes are dispersively coupled to two breath mechanical modes (one can be the radial expansion mode, the other one can be the out-of-plain vibration mode). In the bosonic four-mode system, the CW (CCW) optical mode is driven by lasers at two frequencies $\omega_{c,k} - \omega_{m1}$ and $\omega_{c,k} - \omega_{m2}$, with different amplitudes and phases. Under the condition that $\min[\omega_{m1},\ \omega_{m2},\ |\omega_{m1} - \omega_{m2}|] \gg \max[\kappa,\ \gamma_{m1},\ \gamma_{m2}]$, we can realize the coherent coupling between the phonons and photons, the effective interaction Hamiltonian can be written as

$$H_{lin} = \sum_{j=1,2} G_{kj} a_k^\dagger b_{0j} + G_{-kj} a_{-k}^\dagger b_{0j} + H.c., \qquad (11)$$

where b_{0j} $(j = 1, 2)$ is the annihilation operator of the mechanical mode j, and G_{kj} is the effective complex optomechanical coupling with a certain phase from driving fields.

By including the damping effects, the dynamics of the system obeys the quantum Langevin equations

$$\frac{dO}{dt} = -UO + \sqrt{\kappa} O_{in}, \qquad (12)$$

where $O = (a_k,\ a_{-k},\ b_{01},\ b_{02})^T$ is a vector of the operators, the input vector $O_{in} = (\epsilon_{in,k},\ \epsilon_{in,-k},\ 0,\ 0)^T$, and the coefficient matrix

$$U = \begin{pmatrix} \frac{\kappa}{2} & 0 & iG_{k1} & iG_{k2} \\ 0 & \frac{\kappa}{2} & iG_{-k1} & iG_{-k2} \\ iG_{k1}^* & iG_{-k1}^* & \frac{\gamma_{m1}}{2} & 0 \\ iG_{k2}^* & iG_{-k2}^* & 0 & \frac{\gamma_{m2}}{2} \end{pmatrix}. \qquad (13)$$

Transforming the equations into the frequency domain, the intracavity field is solved as $O = (U - i\omega I)^{-1} \sqrt{\kappa} O_{in}$. Using the standard input-output theory $O_{out} = \sqrt{\kappa} O - O_{in}$, the output of the system is obtained as $O_{out} = RO_{in}$, where the scattering matrix $R = \kappa (U - i\omega I)^{-1} - I$. We notice that there are two paths of the coherent conversion between CW and CCW signal photons, therefore the total phase difference θ between the path $a_k \rightleftarrows b_1 \rightleftarrows a_{-k}$ and the path $a_k \rightleftarrows b_2 \rightleftarrows a_{-k}$ plays a key role in the optical mode conversion. When the symmetry between the two paths is broken, the system becomes non-reciprocal.

To illustrate the phase-controlled non-reciprocity, we assume the effective coupling strengths are real except for $G_{k2} = |G_{k2}| e^{i\theta}$. For the convenience of expression, we define the cooperativity $C = \frac{4|G^2|}{\kappa\gamma}$. If only one mechanical mode is coupled to the optical modes, it has been demonstrated in the experiment that the transmission is non-reciprocal only if $C_{k1} \neq C_{-k1}$, while the signal

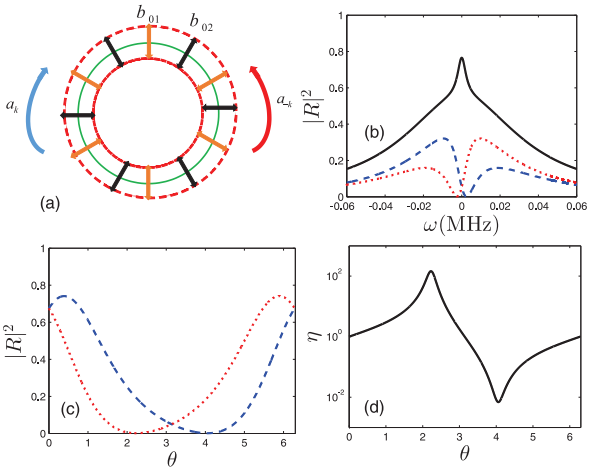

FIG. 3: (Color online) Optical mode conversion between CW and CCW fields. (a) Schematic diagram of phase-controlled nonreciprocity. (b) The conversion efficiency for the reciprocity $\theta = 0$ (the black solid line $|R_{k,-k}|^2 = |R_{-k,k}|^2$) and nonreciprocity $\theta = 3\pi/4$ (the blue dashed line $|R_{k,-k}|^2$and the red dotted line $|R_{-k,k}|^2$) as the function of the signal frequency ω. The conversional probabilities (c) and conversional ratio η (d) as the function of the phase θ for the frequency $\omega = -\gamma_{m2}$. The other parameters are $C_{k1} = C_{-k1} = 1$, $C_{k2} = C_{-k2} = 2.5$, $G_{k2} = |G_{k2}|e^{i\theta}$, $\kappa/2\pi = 15$ MHz, $\gamma_{m1}/2\pi = 22 \times 10^{-3}$MHz, and $\gamma_{m2}/2\pi = 22 \times 10^{-4}$MHz.

reflection is always reciprocal [47]. In additional to the optomechanically induced phase shifting and absorption, the non-reciprocal conversion between two modes is also very important for information processing, and this can be realized in our scheme.

The Fig. 3(b-d) shows the conversion efficiencies between CW and CCW modes as a function of the signal frequency ω and the pump phase differences θ. The black solid line in the Fig. 3(b) shows the reciprocal conversion when the phase $\theta = 0$. However, when we choose the phase $\theta = 3\pi/4$, as shown in Fig. 3(b), the nonreciprocal conversion $|R_{k,-k}|^2 \neq |R_{-k,k}|^2$ is observed. When $\omega \approx -\gamma_{m2}$, we find $|R_{-k,k}|^2 \to 0$ (the red dotted line), which means that the conversion from the CW to the CCW is almost forbidden, while the opposite conversion is feasible. When $\omega \approx \gamma_{m2}$, there is an opposite result, which is confirmed by the blue dashed line $|R_{k,-k}|^2$. To further illustrate the effect of the phase, we plot the conversion efficiency as the function of the phase θ for the frequency $\omega = -\gamma_{m2}$ in the Fig. 3(c), which obviously shows that the optical conversion can be periodically changed with the increasing of the phase θ. Fig. 3(d) shows the ratio $\eta = |R_{k,-k}|^2 / |R_{-k,k}|^2$as the function of the phase θ, which can reach the nonreciprocal degree $\eta \propto 10^2$ for the experimental parameters. It is obvious that the total phase difference θ plays a key role in the optical mode conversion.

If we can realize the parameters $\gamma_{m2} \ll G \sim \kappa \ll \gamma_{m1}$, the ideal non-reciprocal optical conversion is possible. This assumption seems to be counter-intuitive because usually the damping rate of the mechanical mode is smaller than the decay rate of the cavity mode, but we can satisfy the condition when the mechanical mode is coupled to an auxiliary cavity mode [60]. In addition, the signal frequency ω of ideal optical conversion can be tuned by the detuning between the driving fields and the optical modes, which has been recently demonstrated in the microwave transmission [61].

V. PHONONIC PARITY-TIME SYMMETRY

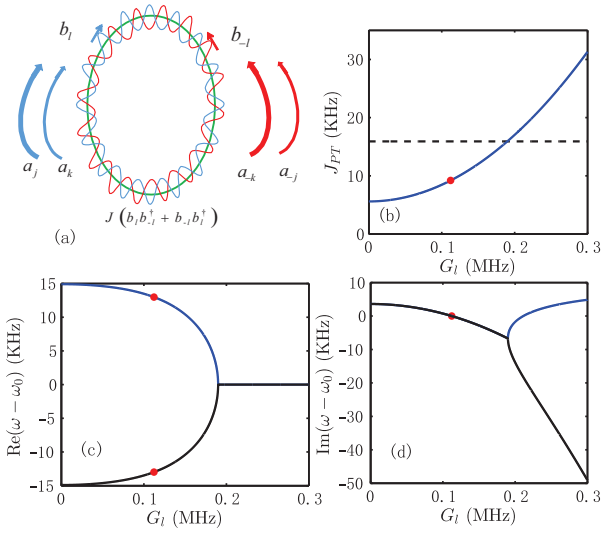

FIG. 4: (Color online) PT-symmetry in deformation optomechanical system. (a) Schematic diagram of PT-symmetry. The threshold coupling strength J_{PT} (b), the real Re(ω) (c) and Im(ω) (d) versus the G_l. The black dash line in (b) shows the coupling $J/2\pi = 16$ KHz. The red dots means that gain and loss are balanced (i.e., $\gamma_{-l} + \gamma_m = -\gamma_l - \gamma_m$), which is the ideal PT-symmetry. The parameters are $\omega_{ml}/2\pi = 42.3$ MHz, $\gamma_m/2\pi = 4$ KHz, $G_{-l}/2\pi = 0.14$ MHz, $J/2\pi = 16$ KHz, and $\kappa_1/2\pi = \kappa_2/2\pi = 3.5$ MHz.

Most of previous studies are focus on the control of multiple optical signal modes. The degenerate CW and CCW acoustic modes can also be used for interesting applications. Here, we consider a stimulated Brillouin scattering in this triple-resonant optomechanics [49, 50], in which the Hamiltonian can be described as

$$H_{sbs} = \sum_{o=j,k} \omega_{c,o} a_o^\dagger a_o + \omega_{ml} b_l^\dagger b_l + g_{j,k,l}\left(b_l^\dagger a_j^\dagger a_k + H.c\right), \tag{14}$$

where a_j, a_k are the optical modes and b_l is the acoustic mode that satisfies the selection rule.

In a perfect rotational symmetric whispering-gallery microresonator, the CW and CCW acoustic modes are

degenerate. To study the non-Hermitian physics of the phononic mode, we consider a slightly deformed microresonator that breaks the rotational symmetry and induces an effective coupling between b_l and b_{-l}. The schematic of the system is shown in the Fig. 4(a), and the phonon coupling is described as

$$H_{bs} = J(b_l^\dagger b_{-l} + b_l b_{-l}^\dagger), \tag{15}$$

where J is the deformed boundary induced backscattering, i.e. the coupling between the mechanical CW and CCW modes. In practical experimental system, the J can be easily controlled to be the order of γ_m without degrading the high quality factor of optical and mechanical modes. Since the optical wavelength is much shorter than that of acoustic modes, the smooth boundary deformation will not induce observable backscattering between the optical modes.

If we drive the optical mode a_j for the CW direction and a_{-k} for the CCW direction by two control fields, the Hamiltonian can be simplified as

$$\begin{aligned} H_{lin} =& H_0 + J(b_l^\dagger b_{-l} + b_l b_{-l}^\dagger) \\ &+ \left(G_l a_k^\dagger b_l + G_{-l} a_{-j} b_{-l} + H.c\right), \end{aligned} \tag{16}$$

where $G_{l(-l)} = g_{j,k,l}\alpha_{j(-k)}$ is the effective optomechanical coupling by the driving field $\alpha_{j(-k)}$.The Hamiltonian $H_0 = \Delta_k a_k^\dagger a_k + \Delta_{-j} a_{-j}^\dagger a_{-j} + \omega_{ml}\left(b_l^\dagger b_l + b_{-l}^\dagger b_{-l}\right)$, in which $\Delta_k = \omega_{c,k} - \omega_{j,l}$ and $\Delta_{-j} = \omega_{c,j} - \omega_{-\mathrm{k},l}$, where $\omega_{j,l}$ and $\omega_{-k,l}$ are the frequencies driving on a_j and a_{-k}, respectively.

To investigate the PT-symmetric mechnaical system [62, 63], we use a probe field to drive the optical mode a_{-j} with the frequency ω_p. We can write the following rate equations for the coupled-resonators system

$$\frac{dO}{dt} = -UO + \sqrt{\kappa_{in}} O_{in}, \tag{17}$$

where $O = \left(a_k,\ a_{-j}^\dagger,\ b_l,\ b_{-l}\right)^T$ is a vector of the operators, the input vector $O_{in} = (0,\ \epsilon_p,\ 0,\ 0)^T$, and the coefficient matrix

$$U = \begin{pmatrix} i\delta_k + \frac{\kappa_2}{2} & 0 & iG_l & 0 \\ 0 & -i\delta_{-j} + \frac{\kappa_1}{2} & 0 & -iG_{-l} \\ iG_l & 0 & i\delta_l + \frac{\gamma_m}{2} & iJ \\ 0 & iG_{-l} & iJ & i\delta_{-l} + \frac{\gamma_m}{2} \end{pmatrix}, \tag{18}$$

where $\delta_k = \Delta_k + \omega_p - \omega_{-k,l}$, $\delta_{-j} = \omega_{c,j} - \omega_p$, $\delta_l = \omega_{ml} + \omega_p - \omega_{-k,l}$, $\delta_{-l} = \delta_l$. For $\kappa_{1,2} \gg \gamma_\mathrm{m}$, we can adiabatically eliminate the optical modes by

$$a_{-j}^\dagger = \frac{iG_{-l} b_{-l} + \sqrt{\kappa_{in}}\epsilon_p}{-i\delta_{-j} + \frac{\kappa_1}{2}}, \tag{19}$$

$$a_k = \frac{-iG_l b_l}{i\delta_k + \frac{\kappa_2}{2}}, \tag{20}$$

and we can obtain the effective rate equations of the acoustic modes

$$\begin{aligned} \frac{db_l}{dt} &= -\left(i\delta_l + \frac{\gamma_m}{2} + \frac{G_l^2}{i\delta_k + \frac{\kappa_2}{2}}\right) b_l \\ &\quad -iJb_{-l}, \end{aligned} \tag{21}$$

$$\begin{aligned} \frac{db_{-l}}{dt} &= -\left(i\delta_{-l} + \frac{\gamma_m}{2} - \frac{G_{-l}^2}{-i\delta_{-j} + \frac{\kappa_1}{2}}\right) b_{-l} \\ &\quad -iJb_l - \frac{iG_{-l}\sqrt{\kappa_{in}}\epsilon_p}{-i\delta_{-j} + \frac{\kappa_1}{2}}. \end{aligned} \tag{22}$$

Here we choose the driving frequency $\omega_{-k,l} = \omega_{c,k}$ and $\omega_{j,l} = \omega_{c,j} = \omega_p$. The coupling of these two resonators creates two supermodes $B_+ = (b_l + b_{-l})/\sqrt{2}$ and $B_- = (b_{-l} - b_l)/\sqrt{2}$ with the eigenfrequencies ω_+ and ω_- given as

$$\omega_\pm = \omega_0 - \frac{i}{4}(2\gamma_m + \gamma_{-l} + \gamma_l) \pm \frac{1}{4}\sqrt{16J^2 - (\gamma_{-l} - \gamma_l)^2}. \tag{23}$$

where $\gamma_{-l} = -\frac{4G_{-l}^2}{\kappa_1}$, $\gamma_l = \frac{4G_l^2}{\kappa_2}$, and $\omega_0 = \frac{\delta_l + \delta_{-l}}{2}$.

Then the value of J sastisfying $16J^2 = (\gamma_{-l} - \gamma_l)^2$ is the threshold coupling strength J_{PT}, which is found as

$$J_{PT} = \frac{1}{4}\left|\gamma_{-l} - \gamma_l\right|. \tag{24}$$

It is clear that J_{PT} depends on the drving strength of the system. For the ideal case when gain and loss are balanced (i.e., $\gamma_{-l} + \gamma_\mathrm{m} = -\gamma_l - \gamma_\mathrm{m}$), the coupling strength J_{PT} becomes

$$J_{PT} = \frac{\gamma_l + \gamma_\mathrm{m}}{2}. \tag{25}$$

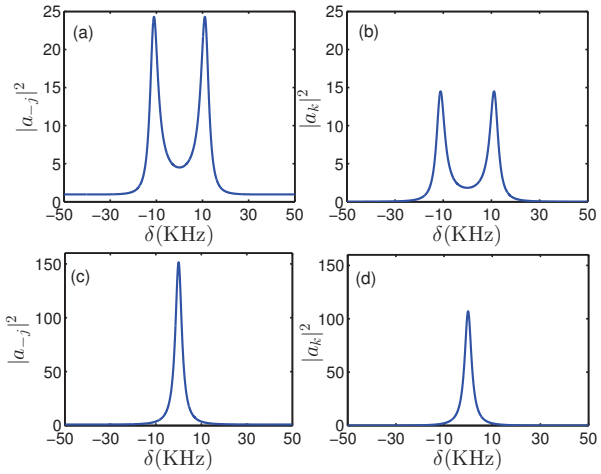

FIG. 5: The spectra as the function of the detuning δ. (a) $|a_{-j}|^2$ and (b) $|a_k|^2$ with $G_l/2\pi = 0.14$ MHz. We have $J_{PT} < J$, which is related to the unbroken-PT-symmetry. (c) $|a_{-j}|^2$ and (d) $|a_k|^2$ show the broken-PT-symmetry for $J_{PT} > J$ with $G_l/2\pi = 0.2$ MHz. Other parameters are the same as the above.

The threshold coupling strength J_{PT} versus the G_l for the fixed $G_{-l}/2\pi = 0.14$ MHz is plotted in the Fig. 4(b). The black dash line shows the coupling $J/2\pi = 16$ kHz and the red dot is corresponding to the ideal PT-symmetry. For $J_{PT}/J < 1$, the system is in a unbroken-symmetry phase in Fig. 4(c) and 4(d), as seen in both the non-zero difference of the real parts of the eigenfrequencies and the coalescence in their imaginary parts. As J_{PT}/J approaches 1 from below, the difference in the real parts of the eigenfrequencies decreases and their imaginary parts bifurcate.

To observe the phenomena of the PT-symmetry, we can calculate the intracavity field by the Eq. (17). When the system is in the steady state $\frac{dO}{dt} = 0$, we obtain

$$a_k = \frac{-iG_l b_l}{i\delta + \kappa_2/2}, \tag{26}$$

$$a_{-j}^{\dagger} = \frac{iG_{-l} b_{-l} + \sqrt{\kappa_{in}}\epsilon_p}{i\delta + \frac{\kappa_1}{2}}, \tag{27}$$

$$b_l = \frac{iJb_{-l}}{F_2(\delta)}, \tag{28}$$

$$b_{-l} = \frac{iG_{-l}\sqrt{\kappa_{ex}}\epsilon_p}{i\delta + \frac{\kappa_1}{2}} \Big/ \left[F_1(\delta) + \frac{J^2}{F_2(\delta)}\right], \tag{29}$$

where $F_1(\delta) = -i\delta - \frac{\gamma_m}{2} + \frac{G_{-l}^2}{i\delta + \frac{\kappa_1}{2}}$ and $F_2(\delta) = -i\delta - \frac{\gamma_m}{2} - \frac{G_l^2}{i\delta + \kappa_2/2}$, in which the detuning $\delta = \omega_p - \omega_{c,j}$.

The spectra of the steady-state intracavity field are shown in Fig. 5. When we choose the coupling $G_l/2\pi = 0.14$ MHz, we have the threshold coupling strength $J_{PT} < J$, which is in the unbroken-PT-symmetric region. Fig. 5(a) shows the intracavity field $|a_{-j}|^2$ as the function of detuning δ, and there are two resonance peaks, which are corresponding to non-zero difference of the real parts of the eigenfrequencies in the Fig. 4(b). The imaginary parts of the eigenfrequencies in Fig. 4(c) show the coalescence, which is confirmed with the same width of the two peaks. The intracavity field $|a_k|^2$ is plotted in the Fig. 5(b), which shows the similar phenomena. When $J_{PT} > J$ with the coupling $G_l/2\pi = 0.2$ MHz, we observe the broken-PT-symmetric phenomena, and there is one peak in the Fig. 5(c) and 5(d). By the deformation optomechanical system, we demonstrate that the parity-time symmetry of acoustic modes can be observed. More importantly, gain could be provided only by optical fields without nonlinear processes. Based on parameters realized with existing technology in recent experiments, these optomechanical devices should be readily achievable.

The parameters we choose above satisfy $\mathrm{Im}(\omega - \omega_0) < 0$, which means that all modes have the loss. When $\mathrm{Im}(\omega - \omega_0) > 0$, it is obvious that the system is unstable, and we can calculate the intracavity field with driving pulse numerically by the Eq. (17). In the linear regime, the transmission is reciprocal regardless of whether the symmetry is broken or unbroken.

VI. DISCUSSION

The traveling-wave optomechanical system can be realized in the solid state whispering gallery microresonators, with various shapes and materials [64]. Those high-quality materials usually support not only high quality factor (Q) optical modes, but also supports high Q mechanical modes. Especially, in polished single crystal resonators, the mechanical quality factor can be as high as 10^5 [65]. Therefore, this type microresonator has great potential for the coherent optomechanical interactions.

Compared with the optical modes, the mechanical modes have much longer lifetime and can be used as quantum memory. In compare with the usual single mode optomechanics, the traveling-wave microresoantors have two unique advantages, the mode degeneracy and suppression of dephasing. By employing the degenerate CW and CCW acoustic modes, the binary bosonic memory is possible [50]. The degenerate traveling modes have the remarkable properties that the modes bear the same noise source, and the noises cancel in most of applications. For example, if a single phonon excitation is stored as a superposition of CW and CCW directions, their phase coherence can be insensitive to the external vibration and thermal noise. Because the dominated dephasing noise of both CW and CCW are the same, the relative phase between CW and CCW mode conserves. Therefore, the natural degenerate modes in traveling-wave microresonators form a decoherence-free subspace and preserve the coherence.

In practical applications, the degeneracy of the CW and CCW modes would also save the laser source. We can use one pump laser to study the coherent interaction in two directions. Besides the CW and CCW modes studied in this work, the traveling-wave optomechanical system supports optical modes and mechanical modes in a large frequency range, with the mode frequency approximately proportional to the angular momentum $|l|$. By choosing a proper material, there will be hundreds of optical modes covering the visible, IR and mid-IR frequency range. Similarly, the acoustic wave modes also show a comb like spectrum, and have the frequency range from few MHz to GHz [66]. So, the applications discussed in this paper on the CW and CCW modes can be generalized to the modes with very different frequencies.

VII. CONCLUSION

In summary, we theoretically study the multimode optomechanics based on the traveling-wave microresonators, where the degenerate clockwise and counterclockwise optical and acoustical modes can be controlled selectively by optically pumping in different directions. By the unique properties of the traveling-wave optomechanic systems, we have proposed several unique applications of the system. Based on the parameters realized in recent experiments, these optomechanical devices should

be readily achievable, even on the level of single-photon with practical noises.

Acknowledgments. We thank Yuan Chen for preparing figure 1b and 1c, and acknowledge Chuan-Shen Yang and Hui Jing for useful suggestions. This work was funded by the National Key R & D Program (Grant No. 2016YFA0301300, and 2016YFA0301700), and the National Natural Science Foundation of China (Grant No. 11474271 and Grant No. 11674305), the China Postdoctoral Science Foundation (No. 2016M602013). YDW acknowledges the support of NSFC grant No. 11574330 and No. 11434011.

[1] M. Aspelmeyer, T. J. Kippenberg, and F. Marquardt, Cavity optomechanics, Rev. Mod. Phys. **86**, 1391 (2014).
[2] T. J. Kippenberg and K. J. Vahala, Cavity Optomechanics: Back-Action at the Mesoscale, Science **321**, 1172 (2008).
[3] M. Aspelmeyer, P. Meystre, and K. Schwab, Quantum optomechanics, Phys. Today **65**, 29 (2012).
[4] D. Van Thourhout and J. Roels, Optomechanical device actuation through the optical gradient force, Nat. Photon. **4**, 211 (2010).
[5] T. Hong, H. Yang, H. Miao, and Y. Chen, Open quantum dynamics of single-photon optomechanical devices, Phys. Rev. A **88**, 023812 (2013).
[6] M. Li, W. H. P. Pernice, C. Xiong, T. Baehr-Jones, M. Hochberg, and H. X. Tang, Harnessing optical forces in integrated photonic circuits, Nature **456**, 480 (2008).
[7] M. Eichenfield, R. Camacho, J. Chan, K. J. Vahala, and O. Painter, A picogram- and nanometre-scale photonic-crystal optomechanical cavity, Nature **459**, 550 (2009).
[8] L. Fan, C.-L. Zou, M. Poot, R. Cheng, X. Guo, X. Han, and H. X. Tang, Integrated optomechanical single-photon frequency shifter, Nat. Photonics **10**, 766–770 (2016).
[9] M. Bagheri, M. Poot, M. Li, W. P. H. Pernice, and H. X. Tang, Dynamic manipulation of nanomechanical resonators in the high-amplitude regime and non-volatile mechanical memory operation, Nat. Nanotechnol. **6**, 726 (2011).
[10] G. D. Cole, and M. Aspelmeyer, Cavity optomechanics: Mechanical memory sees the light, Nat. Nanotechnol. **6**, 690 (2011).
[11] G. Anetsberger, E. Gavartin, O. Arcizet, Q. P. Unterreithmeier, E. M. Weig, M. L. Gorodetsky, J. P. Kotthaus, and T. J. Kippenberg, Measuring nanomechanical motion with an imprecision below the standard quantum limit, Phys. Rev. A **82**, 061804 (2010).
[12] P. Weber, J. Güttinger, A. Noury, J. Vergara-Cruz , and A. Bachtold, Force sensitivity of multilayer graphene optomechanical devices, Nat. Commun. **7**, 12496 (2016).
[13] C. F. Ockeloen-Korppi, E. Damskägg, J.-M. Pirkkalainen, A. A. Clerk, M. J. Woolley, and M. A. Sillanpää, Quantum Backaction Evading Measurement of Collective Mechanical Modes, Phys. Rev. Lett. **117**, 140401 (2016).
[14] J. Aasi et al., Enhanced sensitivity of the LIGO gravitational wave detector by using squeezed states of light, Nat. Photon. **7**, 613 (2013).
[15] A. Belenchia, D. M. T. Benincasa, S. Liberati, F. Marin, F. Marino, and A. Ortolan, Testing Quantum Gravity Induced Nonlocality via Optomechanical Quantum Oscillators, Phys. Rev. Lett. **116**, 161303 (2016).
[16] M. Ludwig, B. Kubala, and F. Marquardt, The optomechanical instability in the quantum regime, New J. Phys. **10**, 095013 (2008).
[17] F. Brennecke, S. Ritter, T. Donner, T. Esslinger, Cavity Optomechanics with a Bose-Einstein Condensate, Science **322**, 235 (2008).
[18] F. Khalili, S. Danilishin, H. Miao, H. Müller-Ebhardt, H. Yang, and Y. Chen, Preparing a Mechanical Oscillator in Non-Gaussian Quantum States, Phys. Rev. Lett. **105**, 070403 (2010).
[19] K. Stannigel, P. Komar, S. J. M. Habraken, S. D. Bennett, M. D. Lukin, P. Zoller, and P. Rabl, Optomechanical Quantum Information Processing with Photons and Phonons, Phys. Rev. Lett. **109**, 013603 (2012).
[20] T. P. Purdy, R. W. Peterson, and C. A. Regal, Observation of Radiation Pressure Shot Noise on a Macroscopic Object, Science **339**, 801(2013).
[21] J. D. Teufel et al., Sideband cooling of micromechanical motion to the quantum ground state, Nature **475**, 359 (2011).
[22] S. Weis, R. Rivière, S. Deléglise, E. Gavartin, O. Arcizet, A. Schliesser, and T. J. Kippenberg, Optomechanically Induced Transparency, Science **330**, 1520 (2010).
[23] A. H. Safavi-Naeini, T. P. Mayer Alegre, J. Chan, M. Eichenfield, M. Winger, Q. Lin, J. T. Hill, D. E. Chang, and O. Painter, Electromagnetically induced transparency and slow light with optomechanics, Nature **472,** 69 (2011).
[24] T. A. Palomaki, J. D. Teufel, R. W. Simmonds, and K. W. Lehnert, Entangling Mechanical Motion with Microwave Fields, Science **342**, 710 (2013).
[25] E. E. Wollman, C. U. Lei, A. J. Weinstein, J. Suh, A. Kronwald, F. Marquart, A. A. Clerk, and K. C. Schwab, Quantum squeezing of motion in a mechanical resonator, Science **349**, 952 (2015).
[26] C. Dong, V. Fiore, M. C. Kuzyk, and H. Wang, Optomechanical Dark Mode, Science **338**, 1609 (2012).
[27] R. W. Andrews, R. W. Peterson, T. P. Purdy, K. Cicak, R. W. Simmonds, C. A. Regal, and K. W. Lehnert, Bidirectional and efficient conversion between microwave and optical light, Nat. Phys. **10**, 321 (2014).
[28] X.-W. Xu and Y. Li, Optical nonreciprocity and optomechanical circulator in three-mode optomechanical systems, Phys. Rev. A **91**, 053854 (2015).
[29] A. Meltelmann and A. A. Clerk, Nonreciprocal Photon Transmission and Amplification via Reservoir Engineering, Phys. Rev. X **5**, 021025 (2015).
[30] V. Peano, M. Houde, C. Brendel, F. Marquardt, and A. A. Clerk, Topological phase transitions and chiral inelastic transport induced by the squeezing of light, Nat. Commun. **7**, 10779 (2016).
[31] B. Peng et al., Parity–time-symmetric whispering-gallery microcavities, Nat. Phys. **10**, 394 (2014).
[32] C. Wurl, A. Alvermann, and H. Fehske, Symmetry-breaking oscillations in membrane optomechanics, Phys. Rev. A **94** 063860 (2016).

[33] H. Xu, D. Mason, Luyao Jiang, and J. G. E. Harris, Topological energy transfer in an optomechanical system with exceptional points, Nature **537**, 80 (2016).

[34] I. S. Grudinin, H. Lee, O. Painter, and K. J. Vahala, Phonon Laser Action in a Tunable Two-Level System, Phys. Rev. Lett. **104**, 083901 (2010).

[35] J. Fan and L. Zhu, Enhanced optomechanical interaction in coupled microresonators, Opt. Express **20**, 20790 (2012).

[36] L. F. Buchmann and D. M. Stamper-Kurn, Nondegenerate multimode optomechanics, Phys. Rev. A **92**, 013851 (2015).

[37] T. Kipf and G. S. Agarwal, Superradiance and collective gain in multimode optomechanics, Phys. Rev. A **90**, 053808 (2014).

[38] S. Chesi, Y. D. Wang, and J. Twamley, Diabolical points in multi-scatterer optomechanical systems, Sci. Rep. **5**, 7816 (2015).

[39] Z. J. Deng, X.-B. Yan, Y.-D. Wang, and C.-W. Wu, Optimizing the output-photon entanglement in multimode optomechanical systems, Phys. Rev. A **93**, 033842 (2016).

[40] Y.-S. Park and H. Wang, Resolved-sideband and cryogenic cooling of an optomechanical resonator, Nat. Phys. **5**, 489 (2009).

[41] K. C. Balram, M. Davanço, J. Y. Lim, J. D. Song, and K. Srinivasan, Moving boundary and photoelastic coupling in GaAs optomechanical resonators, Optica **1**, 414 (2014).

[42] C. Baker, W. Hease, D.-T. Nguyen, A. Andronico, S. Ducci, G. Leo, and I. Favero, Photoelastic coupling in gallium arsenide optomechanical disk resonators, Opt. Express **22**, 14072 (2014).

[43] M. Tomes, F. Marquardt, G. Bahl, and T. Carmon, Quantum-mechanical theory of optomechanical Brillouin cooling, Phys. Rev. A **84**, 063806 (2011).

[44] I. S. Grudinin, A. B. Matsko, and L. Maleki, Brillouin Lasing with a CaF2 Whispering Gallery Mode Resonator, Phys. Rev. Lett. **102**, 043902 (2009).

[45] G. Bahl, J. Zehnpfennig, M. Tomes, and T. Carmon, Stimulated optomechanical excitation of surface acoustic waves in a microdevice. Nat. Commun. **2**, 403 (2011).

[46] G. Bahl, M. Tomes, F. Marquardt, and T. Carmon, Observation of spontaneous Brillouin cooling. Nat. Phys. **8**, 203–207 (2012).

[47] Z. Shen, Y.-L. Zhang, Y. Chen, C.-L. Zou, Y.-F. Xiao, X.-B. Zou, F.-W. Sun, G.-C. Guo, and C.-H. Dong, Experimental realization of optomechanically induced nonreciprocity, Nat. Photon. **10**, 657 (2016).

[48] F. Ruesink, M.-A. Miri, A. Alù, and E. Verhagen, Nonreciprocity and magnetic-free isolation based on optomechanical interactions, Nat. Commun. **7**, 13662 (2016).

[49] J. H. Kim, M C. Kuzyk, K. Han, H. Wang, and G. Bahl, Non-reciprocal Brillouin scattering induced transparency, Nat. Phys. **11**, 275 (2015).

[50] C.-H. Dong, Z. Shen, C.-L. Zou, Y.-L. Zhang, W. Fu, and G.-C. Guo, Brillouin-scattering-induced transparency and non-reciprocal light storage, Nat. Commun. **6**, 6193 (2015).

[51] M. O. Scully and M. S. Zubairy, Quantum Optics (Cambridge Univ. Press, Cambridge, 1997).

[52] G. S. Agarwal, Nonclassical statistics of fields in pair coherent states, J. Opt. Soc. Am. B **5**, 1940 (1988).

[53] Girish S. Agarwal, Quantum Optics (Cambridge Univ. Press, Cambridge, 2013).

[54] E. X. DeJesus and C. Kaufman, Routh-Hurwitz criterion in the examination of eigenvalues of a system of nonlinear ordinary differential equations, Phys. Rev. A **35**, 5288 (1987).

[55] C. Simon, H. de Riedmatten, M. Afzelius, N. Sangouard, H. Zbinden, and N. Gisin, Quantum Repeaters with Photon Pair Sources and Multimode Memories, Phys. Rev. Lett. **98**, 190503 (2007).

[56] J. Fulconis, O. Alibart, J. L. O'Brien, W. J. Wadsworth, and J. G. Rarity, Nonclassical Interference and Entanglement Generation Using a Photonic Crystal Fiber Pair Photon Source, Phys. Rev. Lett. **99**, 120501 (2007).

[57] Ying-Dan Wang and Aashish A. Clerk, Reservoir-Engineered Entanglement in Optomechanical Systems, Phys. Rev. Lett. **110**, 253601 (2013).

[58] M. Schmidt, M. Ludwig, and F. Marquardt, Optomechanical circuits for nanomechanical continuous variable quantum state processing, New J. Phys. **14**, 125005 (2012).

[59] Lin Tian, Robust Photon Entanglement via Quantum Interference in Optomechanical Interfaces, Phys. Rev. Lett. **110**, 233602 (2013).

[60] Xun-Wei Xu, Yong Li, Ai-Xi Chen, and Yu-xi Liu, Nonreciprocal conversion between microwave and optical photons in electro-optomechanical systems, Phys. Rev. A **93**, 023827 (2016).

[61] N. R. Bernier, L. D. Tóth, A. Koottandavida, A. Nunnenkamp, A. K. Feofanov, T. J. Kippenberg, Nonreciprocal reconfigurable microwave optomechanical circuit, arXiv:1612.08223 (2016).

[62] H. Jing, S. K. Özdemir, X.-Y. Lü, J. Zhang, L. Yang, and F. Nori, PT -Symmetric Phonon Lase, Phys. Rev. Lett. **113**, 053604 (2014).

[63] V. V. Konotop, J. Yang, and D. A. Zezyulin, Nonlinear waves in PT -symmetric systems, Rev. Mod. Phys. **88**, 035002 (2016).

[64] D. V Strekalov, C. Marquardt, A. B. Matsko, H. G. L. Schwefel, and G. Leuchs, Nonlinear and quantum optics with whispering gallery resonators, J. Opt. **18**, 123002 (2016).

[65] X. Zhang, C.-L. Zou, L. Jiang, and H. X. Tang, Cavity magnomechanics, Science Advances **2**, e1501286 (2016).

[66] A. A. Savchenkov, A. B. Matsko, V. S. Ilchenko, D. Seidel, and L. Maleki, Surface acoustic wave optomechanical oscillator and frequency comb generator, Opt. Lett. **36**, 3338–40 (2011).